Zuse Institute Berlin

Takustr. 7
14195 Berlin
Germany

MARTIN WEISER, YVONNE FREYTAG, BODO ERDMANN,
MICHAEL HUBIG, GITA MALL

Optimal Design of Experiments for Estimating the Time of Death in Forensic Medicine

ZIB Report 18-08 (February 2018)

Zuse Institute Berlin
Takustr. 7
14195 Berlin
Germany

Telephone: +49 30-84185-0
Telefax: +49 30-84185-125

E-mail: bibliothek@zib.de
URL: http://www.zib.de

ZIB-Report (Print) ISSN 1438-0064
ZIB-Report (Internet) ISSN 2192-7782

Optimal Design of Experiments for Estimating the Time of Death in Forensic Medicine

Martin Weiser* Yvonne Freytag* Bodo Erdmann*
Michael Hubig† Gita Mall†

March 1, 2018

Abstract

Estimation of time of death based on a single measurement of body core temperature is a standard procedure in forensic medicine. Mechanistic models using simulation of heat transport promise higher accuracy than established phenomenological models in particular in nonstandard situations, but involve many not exactly known physical parameters. Identifying both time of death and physical parameters from multiple temperature measurements is one possibility to reduce the uncertainty significantly.

In this paper, we consider the inverse problem in a Bayesian setting and perform both local and sampling-based uncertainty quantification, where proper orthogonal decomposition is used as model reduction for fast solution of the forward model. Based on the local uncertainty quantification, optimal design of experiments is performed in order to minimize the uncertainty in the time of death estimate for a given number of measurements. For reasons of practicability, temperature acquisition points are selected from a set of candidates in different spatial and temporal locations. Applied to a real corpse model, a significant accuracy improvement is obtained already with a small number of measurements.

1 Introduction

Cooling of corpses after death is the foundation of temperature-based estimation of time of death (ToD) in forensic medicine. This method, applicable within a time frame of about 24 hours after death, is one of the standard procedures performed on crime scenes. Established practice is to take one rectal temperature measurement and to find the point of time at which a phenomenological cooling curve attains the measured value [7]. The widely accepted phenomenological cooling model by Marshall and Hoare is a doubly-exponential curve with four parameters [20], two of which can be fixed from the initial body core temperature of about 37^oC and from physical considerations. A choice of the remaining two parameters based on body mass, environmental temperature, and clothing

*Zuse Institute Berlin, Berlin, Germany
†Institute of Forensic Medicine, Jena University Hospital – Friedrich Schiller University, Jena, Germany

has been proposed by Henßge [11, 12] on the basis of a small number of cases. A somewhat larger set of cases has been established later [22].

A drawback of this approach is that several aspects affecting the cooling of the corpse and hence the time of death estimate, e.g., posture, anatomy, irradiation, and changes in environmental temperature, are not captured in the model. The negligence of such conditions leads to considerable uncertainty in the estimated time of death, in particular in nonstandard situations. Due to ethical restrictions, the acquisition of more data for a better parametrization of phenomenological models is severely limited.

This limitation of phenomenological models can in principle be overcome by mechanistic models obtaining the cooling curve from a detailed simulation of the underlying physical processes, as proposed by Mall et al. [19]. While this allows to capture also nonstandard situations [14,21], mechanistic models contain many parameters such as heat capacities and conductivities, corpse geometry, tissue distribution, and environmental temperatures. Since the parameters' values affect the cooling curve, their accuracy is important for the accuracy of the time of death estimate. Some parameters can be obtained directly, e.g., the corpse's geometry and tissue distribution from computed tomography [30], or the environmental temperature at the time when the body is found. Other parameters are in principle measurable, but their acquisition faces practical problems, e.g., heat capacities of different tissues, or heat transfer coefficients of clothing. Finally there are parameters that are principally unaccessible, such as the time course of environmental temperature before the corpse is found, or the supravital metabolic heat generation. Of course, the parameters have different impact on the rectal temperature curve [31], such that not all need to be known with the same precision.

One possibility to gather more information about those parameters with the most impact on the cooling curve is to take more temperature measurements, at several times or in several spatial locations, or both. A parametrization of the Marshall-Hoare model by a least-squares approach for sequential measurements has been proposed recently [29], as well as averaging time of death estimates obtained independently from several measurements [13]. In the present paper, we consider a similar approach for a mechanistic model. Instead of a single intersection of a cooling curve with the constant measured temperature, a more complex inverse problem has to be solved [15]. Here, the time of death is just one of the parameters to be identified. In a Bayesian setting, the solution of the inverse problem is a posterior joint probability distribution for the parameters, from which a marginal distribution for the ultimately interesting time of death can be obtained. Point estimates such as maximum posterior or conditional mean, together with uncertainty information such as variance can be extracted as a more accessible result of the inversion.

On the one hand, the uncertainty in the result can be expected to decrease with increasing information in form of more temperature measurements. On the other hand, acquiring more data increases the measurement effort on the crime scene and is limited by practical issues such as available time and the desired nondestructivity of data acquisition. With a large set of possible temperature measurement positions in space and time, and a much smaller number of measurements that can be taken on the crime scene, the selection of actual positions and times for taking temperature measurements leads to a problem of optimal design of experiments (DoE), see [3, 16, 27].

In the next section, we briefly review the forward model of body cooling, with the relevant parameters, and discuss issues of finite element discretization. Parameter identification and uncertainty quantification in a Bayesian context is presented in Section 3. As local uncertainty quantification based on Taylor approximations is extremely beneficial for efficient optimal design of experiments, we also investigate the accuracy of approximating posterior probability densities by lognormal distributions. This is done using a Markov-Chain Monte Carlo sampling based on model reduction. Finally, we investigate the use of techniques for optimal design of experiments as a means to define good temperature acquisition points. Due to practical requirements – low measurement effort and nondestructivity of testing – measurement locations are chosen from a predefined set of candidate points.

2 The Forward Model

In this section we briefly recall the mechanistic model of heat transfer, the thermal parameters relevant for body cooling, the acquisition of individual anatomy models, finite element discretization of the heat equation, and simplified models.

Thermal model. The physical model of corpse cooling in the time interval $[0, \infty[$ describes the temperature distribution ϑ by Fourier's law of heat conduction,

$$c\rho\dot{\vartheta} = \operatorname{div}(\kappa\nabla\vartheta), \tag{1}$$

where c is the specific heat capacity, ρ the density, and κ the heat conductivity of the tissue. The influence of supravital metabolic heat generation [31] is rather uncertain but in most cases small. Therefore, we neglected it here for simplicity reasons. We interpret the heat capacity $c\rho$ as a single parameter instead of treating density and specific heat capacity separately.

Heat transfer from the body to the environment across the boundary (skin) is due to conduction/advection and radiation:

$$\mathbf{n}^T\kappa\nabla\vartheta = h(\vartheta_{\text{env}} - \vartheta) + \varepsilon\sigma(\vartheta_{\text{env}}^4 - \vartheta^4). \tag{2}$$

Here, $\mathbf{n}$ is the unit outer normal and h the heat transfer coefficient, ϑ_{env} the environmental temperature, ε the emissivity, and $\sigma = 5.6704 \times 10^{-8}\,\mathrm{Wm^{-2}K^{-4}}$ the Stefan-Boltzmann constant. Several simulations have shown that in the usual range of temperatures (270 K to 310 K) a linearization of the Stefan-Boltzmann radiation term has a negligible impact on the cooling curve and hence on the estimated ToD. For the current study, we therefore assume

$$\mathbf{n}^T\kappa\nabla\vartheta = \gamma(\vartheta_{\text{env}} - \vartheta) \tag{3}$$

with the effective heat transfer coefficient $\gamma = h + 4\varepsilon\sigma\vartheta_{\text{env}}^3$. This includes the possibility of irradiation. There is need for special considerations only in cases where the reference temperature ("sky temperature") for radiation deviates significantly from the environmental temperature ϑ_{env}, see [5].

The initial temperature field of the body $\vartheta_0 = \vartheta(0)$ at time $t = 0$ is assumed to be spatially constant, i.e., $\vartheta_0 = \vartheta_{\text{core}}$, with ϑ_{core} being the body core temperature. A slightly more realistic choice would be the solution of the stationary

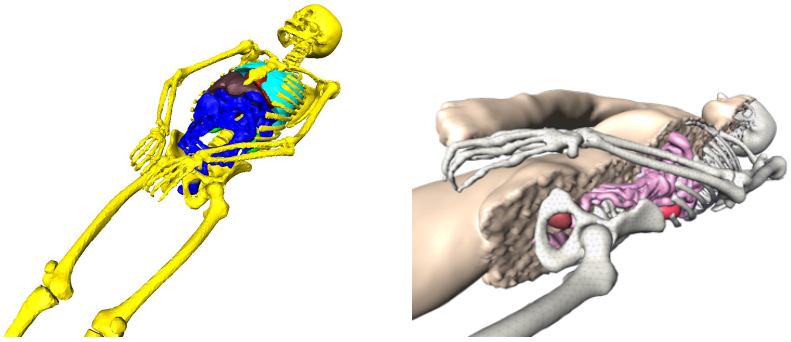

Figure 1: *Left:* Skeleton and inner organs represented in the tetrahedral mesh of the corpse. Muscles, fat, and small intestine are not shown. *Right:* Illustration of tissues in the corpse including muscle, intestine, and fat.

Bio-Heat-Transfer-Equation proposed by Pennes [25],

$$-\operatorname{div}(\kappa\nabla\vartheta_0) + c_b w(\vartheta_0 - \vartheta_{\text{core}}) = 0, \tag{4}$$

where c_b is the heat capacity of blood and w the tissue perfusion. The difference between these two different choices of ϑ_0 has, however, been found to be rather small [31].

Anatomical model. The heat equation (1) is defined on a geometric domain $\Omega \subset \mathbb{R}^3$ representing the corpse. The material parameters $c\rho$, κ, and w depend on the biological tissue type, and are different in particular for muscle, adipose tissue, and bone.

Individual anatomy can be acquired from a CT (computed tomography) scan of the corpse, segmented into the different tissue types. For actual computation, a finite element mesh is created in such a way that a single tissue type can be assigned to each cell [32]. For a sample corpse considered here, the CT data segmented into the nine tissue types bone, fat, muscle, gastrointestinal tract, bladder, kidneys, liver, heart, and lungs is shown in Figure 1. Mesh generation then creates a tetrahedral grid containing $1,439,552$ tetrahedra, and $N = 256,041$ vertices.

Model parameters. The parameters entering into equations (1), (3), and (4) depend on the individual corpse and the environmental conditions at the supposed crime scene. Assigning specific values a priori is therefore subject to some uncertainty, with different impact on the estimated ToD. The uncertainty is considered only for heat capacity and conductivity, but not for perfusion. Sensitivity studies have shown that differentiation of fatty tissue, bones, and tissues with dominant water content such as muscle is sufficient for practical accuracy [31]. Means and standard deviations estimated from various values reported in the literature are given in Table 1.

The assumed values for the remaining parameters are given in Table 2. In particular, we assume a constant environmental temperature ϑ_{env} for simplicity reasons, such that (3) is time invariant. Uncertainty is considered here exemplary for the effective heat transfer coefficient γ only.

Table 1: Averaged thermal properties of human tissues together with estimated standard deviation, condensed from [31].

tissue	$\rho c \pm \sigma_{\rho c}$ 10^6 J/m^3/K	$\kappa \pm \sigma_\kappa$ W/m/K
fat	2.13 ± 0.36	0.21 ± 0.02
bone	2.76 ± 0.48	0.32 ± 0.03
muscle	3.72 ± 0.53	0.49 ± 0.04

Table 2: Global parameters.

parameter	symbol	value	unit
body core temperature	ϑ_{core}	310.15	K
environmental temperature	ϑ_{env}	297.15	K
effective heat transfer coefficient	γ	8.95 ± 0.60	W/m^2/K

Finite element simulation. For a given mesh of the corpse's geometry (including tissue labels per element) and given thermal parameters, the heat transfer model can be solved numerically for the temperature distribution $\vartheta(t)$ by the finite element method, see, e.g., [9,33]. Applying the method of lines to the heat equation (1), (3) yields the linear, high-dimensional, parameter-dependent ordinary equation

$$M\dot{\theta} = A\theta + b, \quad \theta(0) = \theta_0 \tag{5}$$

for the finite element coefficients θ of the temperature distribution $\vartheta = \sum_{i=1}^{N} \theta_i \varphi_i$ in terms of the N finite element basis functions φ_i. Due to the environmental temperature assumed to be constant, the source term b is constant in time.

For the current work, we use the research code Kaskade 7 [10] with linear finite elements and an extrapolated linearly implicit Euler time stepping scheme of order three, and make sure that the numerical discretization error is well below any of the considered modeling errors. Thus, we do not distinguish between the finite element and exact solutions.

3 A Bayesian Approach to Time of Death Estimation

Assume there are m temperature measurements ϑ_i^m, $i = 1, \dots, m$, taken at spatial locations $x_i \in \Omega$ and times t_i. The sequence $(t_i, x_i)_{1 \le i \le m}$ of measurement points will be defined by some protocol specifying $\tau_i = t_i - T \ge 0$ with $\tau_1 = 0$, such that the delay T between death and the first measurement is the time of death.

It will turn out to be convenient in the following to use the parameter vector

$$p := (T, \ln(\rho c_{\text{bone}}), \ln(\rho c_{\text{fat}}), \ln(\rho c_{\text{muscle}}), \ln \kappa_{\text{bone}}, \ln \kappa_{\text{fat}}, \ln \kappa_{\text{muscle}}, \ln \gamma) \in \mathbb{R}^8 \tag{6}$$

containing time of death and the logarithms of the thermal parameters. In terms of this parameter vector, the forward model (5) predicts the temperature

measurement vector as

$$\vartheta_i^m \approx F_i(p) := \vartheta(p + \tau_i e_1, x_i), \quad i = 1, \dots, m,$$

with $e_1 = (1, 0, \dots, 0) \in \mathbb{R}^8$.

In the Bayesian framework [4, 15], both the parameters p and the measurements ϑ^m are assumed to be random variables with associated probability distributions. The *prior* $\pi_{\text{prior}}(p)$ describes the a priori knowledge of parameter values without taking any measurements into account. The *likelihood* $\pi_{\text{like}}(\vartheta^m \mid p)$ is the conditional probability of observing ϑ^m given the parameters p, and describes measurement errors as well as modeling errors. The theorem of Bayes then provides the *posterior* $\pi_{\text{post}}(p \mid \vartheta^m)$, i.e., the conditional probability of parameter values p given that measurements ϑ^m have been observed, as the product

$$\pi_{\text{post}}(p \mid \vartheta^m) \propto \pi_{\text{like}}(\vartheta^m \mid p)\pi_{\text{prior}}(p) \tag{7}$$

up to a normalization constant. From the posterior, point estimates like the maximum posterior parameters $p_{\text{MAP}} = \arg\max \pi_{\text{post}}(p)$ or conditional mean $E[\pi_{\text{post}}]$ together with uncertainty quantification in terms of variance, or marginal densities like the conditional probability $\pi_{\text{post}}(T \mid \vartheta^m)$ of the time of death can be extracted.

3.1 Bayesian inversion

Setting up a Bayesian inverse problem requires to specify the prior and likelihood distributions, which is what we do next.

Prior. Statistical data on thermal tissue properties is scarce due to the difficulties encountered in acquistion and measurement of samples. Rough estimates of mean μ and standard deviation σ can be compiled from available literature as reported in Table 1. Since heat capacities and conductivities as well as heat transfer coefficients are doubtless nonnegative, we assume them to be log-normally distributed [18]:

$$\pi_{\text{prior}}(x) = \Lambda(x; \mu_x^*, \sigma_x^*) = \begin{cases} \frac{1}{\sqrt{2\pi}\sigma_x^*} \exp\left(-\frac{(\ln x - \mu_x^*)^2}{2(\sigma_x^*)^2} - \ln x\right), & x > 0 \\ 0, & x \le 0 \end{cases} \tag{8}$$

for all parameters $x \in \{\rho c_{\text{bone}}, \rho c_{\text{fat}}, \rho c_{\text{muscle}}, \kappa_{\text{bone}}, \kappa_{\text{fat}}, \kappa_{\text{muscle}}, \gamma\}$. The distribution parameters μ^* and σ^* are given in terms of mean μ and standard deviation σ as $\mu^* = \ln \mu - (\sigma^*)^2/2$ and $(\sigma^*)^2 = \ln\left((\sigma/\mu)^2 + 1\right)$. Since then the logarithms are normally distributed with mean $\mu^* - (\sigma^*)^2$ and variance $(\sigma^*)^2$, it is convenient to formulate the inverse problem directly in terms of the logarithms – which is the reason for the definition (6) of the parameter vector p.

The time of death T, however, plays a different role. Usually one knows that T is contained in some interval $[t_a, t_b]$, but nothing else. Among the many noninformative priors that have been proposed [4], we choose the uniform prior for simplicity reasons, and obtain $\pi_{\text{prior}}(T) = (t_b - t_a)^{-1}\chi_{[t_a,t_b]}$.

Lacking any information on statistical dependence, we assume the parameters to be independently distributed, and obtain

$$\pi_{\text{prior}}(p) = \pi_{\text{prior}}(T)\pi_{\text{prior}}(\ln(\rho c_{\text{bone}})) \dots \pi_{\text{prior}}(\ln \gamma). \tag{9}$$

Likelihood. The likelihood describes the distribution of deviations of measurements ϑ^m from model predictions $F(p)$ due to measurement errors and modeling errors. Measurements taken with a single thermal probe contain independent noise as well as a bias due to miscalibration of the thermal probe. Assuming normally distributed errors with standard deviation $\sigma_{\text{noise}} = 0.01\,\text{K}$ and $\sigma_{\text{bias}} = 0.05\,\text{K}$, respectively, we end up with

$$\pi_{\text{like}}(\vartheta^m \mid p) \propto \exp(-(\vartheta^m - F(p))^T \Sigma_l^{-1} (\vartheta^m - F(p))), \tag{10}$$

where $\Sigma_l = \sigma_{\text{noise}}^2 I + \sigma_{\text{bias}}^2 \mathbb{1}\mathbb{1}^T$ and $\mathbb{1} = (1, \ldots, 1)^T \in \mathbb{R}^m$.

Modeling errors such as neglecting the dependence of parameters on temperature, or their spatial variation, are difficult to quantify. We may conjecture that there are neglected effects that affect all measurements in essentially the same way, and other effects that have an independent impact on the measurements. Indeed, some preliminary tests with spatially varying heat capacity and slightly varying location of rectal temperature probe suggest that mainly the bias part is affected, with an effect on the measured temperature in the order of magnitude of 0.1 K. Thus, modeling errors could be taken into account in a very crude way by increasing σ_{bias} to 0.11 K.

Posterior. From (9) and (10) we obtain the posterior distribution as

$$\pi_{\text{post}}(p \mid \vartheta^m) \propto \chi_{[t_a,t_b]}(T) \exp\left(-J(p; \vartheta^m)\right) \tag{11}$$

via the Bayes theorem (7), with the least squares functional

$$J(p; \vartheta^m) = \frac{1}{2}\|\vartheta^m - F(p)\|^2_{\Sigma_l^{-1}} + \frac{1}{2}\|p - (\mu^* - (\sigma^*)^2)\|^2_{\Sigma_p^{-1}} \tag{12}$$

and the prior information matrix $\Sigma_p^{-1} := \text{diag}(0, (\sigma^*_{\rho c_{\text{bone}}})^{-2}, \ldots, (\sigma^*_\gamma)^{-2})$.

Due to monotonicity of the exponential function, maximum posterior points can be computed efficiently by solving the regularized, constrained least squares problem

$$p_{\text{MAP}}(\vartheta^m) = \arg\min_{p \in \mathbb{R}^8_+} J(p; \vartheta^m) \quad \text{subject to} \quad T \in [t_a, t_b]$$

with gradient based methods, e.g., Gauss-Newton methods [8].

Alternatively, the complete posterior distribution π_{post} can be approximated by a sampling generated by, e.g., the Metropolis-Hastings algorithm [15]. The sample mean can then be used as an approximation of the conditional mean point estimate p_{CM}.

Local uncertainty quantification. While posterior sampling provides a direct uncertainty quantification in terms of the sample covariance, the drawback is that many samples are required for obtaining reliable values. Moreover, derivatives of the covariance with respect to the measurement locations and times are difficult to compute, which is a severe drawback in view of the optimal design of experiments considered in Secion 4. In contrast, the maximum posterior point estimate is easily computed, but needs to be complemented by some information on its reliability, such as statistical moments.

If F were linear in p, and $\pi_{\text{prior}}(T)$ Gaussian, the posterior were Gaussian, and its covariance matrix

$$\Gamma(\vartheta^m) = J''(p_{\text{MAP}}(\vartheta_m); \vartheta^m)^{-1} = \left((F')^T \Sigma_l^{-1} F' + \Sigma_p^{-1}\right)^{-1} \tag{13}$$

a complete description of the estimation uncertainty.

Unfortunately, since $\pi_{\text{prior}}(T)$ is uniform and therefore non-Gaussian, and F is nonlinear, the posterior will in general not be Gaussian. Still, if it is unimodal and sufficiently similar to a normal distribution, and T_{MAP} is well in the interior of the interval $[t_a, t_b]$, the covariance approximation

$$\Gamma(\vartheta^m) = J''(p_{\text{MAP}}; \vartheta^m)^{-1} \tag{14}$$

provides a good description of the point estimate's uncertainty.

Among the many criteria for quantifying uncertainty in terms of the posterior covariance [27], the ultimate criterion of interest is the standard deviation $\sigma_T := \Gamma(\vartheta^m)_{TT}^{1/2}$ of the marginal time of death posterior distribution

$$\pi_{\text{post}}(T|\vartheta^m) = \int_{\hat{p}\in\mathbb{R}^7_+} \pi_{\text{post}}((T,\hat{p})|\vartheta^m)\, dx \propto \exp\left(-\frac{(T - T_{\text{MAP}})^2}{2\Gamma_{TT}}\right),$$

a particular case of C-optimality.

It is straightforward to compute not only its value, but also derivatives with respect to the measurement locations and times. This makes local uncertainty quantification particularly attractive for optimal design of experiments. In order to justify its use, we investigate the similarity of the posterior to a normal distribution next.

3.2 Posterior sampling

We consider an artificial setup with the corpse anatomy shown in Figure 1, $t_a = 0$, $t_b = 20\,\text{h}$, and parameters p drawn randomly from the prior π_{prior}. Simulated temperature measurements ϑ^m are simulated at two spatial positions (rectal and skin surface) at four times $\tau_i = 20(i-1)\,\text{min}$, $i = 1, \ldots, 6$, and shifted by measurement errors drawn from the likelihood distribution.

For this setting, a sampling of the posterior can be computed using the Metropolis-Hastings algorithm [15]. Since reasonably accurate representations of the posterior density require many samples, and each evaluation of the posterior involves the solution of the heat equation (5), a really fast solver is needed. Therefore, standard time stepping on the full finite element model is inappropriate.

Model reduction. Using a small, problem-adapted basis for the Galerkin method of lines instead of the large finite element basis is a straightforward way to obtain spatial discretizations of smaller size. In particular for the heat equation, where spatially high-frequent components are damped out quickly, the dimension reduction factor can be expected to be large.

The chosen basis needs to be able to represent arising temperature distributions in the corpse with sufficient accuracy for any parameter value p of potential interest. One way to define such a basis is proper orthogonal decomposition (POD) [17, 26]. In a preprocessing phase, the heat equation (5) is solved for a

Table 3: Parameter values for which snapshots are calculated.

ρc_{bone} J/m^3/K	ρc_{fat} J/m^3/K	ρc_{muscle} J/m^3/K	κ_{bone} W/m/K	κ_{fat} W/m/K	κ_{muscle} W/m/K	γ W/m^2/K
2.76 e+06	2.13 e+06	3.72 e+06	0.32	0.21	0.49	8.95
3.24 e+06	1.82 e+06	3.26 e+06		0.19	0.45	8.39
	2.49 e+06	4.25 e+06		0.23	0.53	9.55

sampling of parameter values, and snapshots of the temperature distribution are taken at several times through the integration. A principal component analysis of these snapshots is then performed to select the n dominant modes $(v_i)_{i=1,\dots,n}$ of variation in the snapshots, and these modes are taken as basis vectors.

For the current setup, finite element solutions have been computed on a cartesian grid on the parameter box for p of width roughly 2σ around the mean value in each parameter dimension as given in Table 3. The number of grid points in each parameter dimension has been chosen according to the relative sensitivity of the time of death estimation with respect to that parameter, resulting in 486 evaluation points. Every 20 min a snapshot has been recorded.

From the principal component analysis, the dominant $n = 10$ modes have been selected. The L^∞ deviation from the finite element solution is quite independent of the actual value in the parameter box, and decreases with time, from around 0.43 K at 6 h to about 0.17 K at 14 h. Mean squared error and the error at selected measurement points are, of course, smaller. For actual estimation of the time of death, the model reduction error of $n = 10$ appears to be too high, and more modes or the full FE model should be used. For the purpose of investigating the global shape of the posterior density, however, and also for design of experiments in Section 4 below, the reduced model can be expected to be accurate enough, in particular as the approximation error is spatially and temporally smooth.

The parameter-dependent mass and stiffness matrices in the discretized heat equation (5) are represented as

$$M = M_0 + \rho c_{\text{bone}} M_{\text{bone}} + \rho c_{\text{fat}} M_{\text{fat}} + \rho c_{\text{muscle}} M_{\text{muscle}} \in \mathbb{R}^{N\times N}$$

and

$$A = A_0 + \kappa_{\text{bone}} A_{\text{bone}} + \kappa_{\text{fat}} A_{\text{fat}} + \kappa_{\text{muscle}} A_{\text{muscle}} + \gamma A_\gamma \in \mathbb{R}^{N\times N},$$

respectively, which is possible due to the linearity of the equation. With the Galerkin prolongation matrix V containing the n dominant modes as columns, the reduced model contains the mass matrix

$$\bar{M} = V^T M V = V^T M_0 V + \sum_{i\in\{\text{bone,fat,muscle}\}} \rho c_i V^T M_i V \in \mathbb{R}^{n\times n},$$

and the reduced stiffness matrix $\bar{A} \in \mathbb{R}^{n\times n}$ defined analogously, as well as the source vector $\bar{b} = V^T b$. The reduced ODE model for the POD coefficients $\theta \in \mathbb{R}^n$ then has the same structure as (5),

$$\bar{M}\dot{\theta} = \bar{A}\theta + \bar{b}, \quad \theta(0) = \theta_0 = \vartheta_0 V^T \mathbb{1}, \tag{15}$$

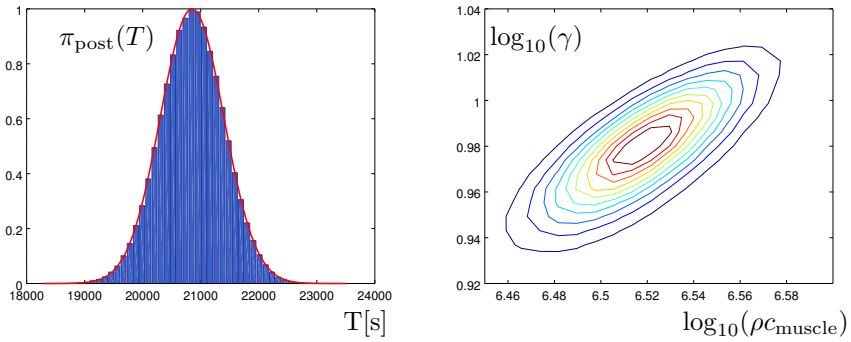

Figure 2: Marginal posterior distributions estimated from the sampling S. *Left:* Histogram of the posterior $\pi_{\text{post}}(T)$ of the time of death T together with a Gaussian of same mean and variance, both scaled to maximum 1. *Right:* Contour lines of a histogram with 30×30 bins of the marginal posterior for muscle heat capacity ρc_{muscle} and surface heat transfer coefficient γ.

where $\mathbb{1} = (1, \dots, 1)^T \in \mathbb{R}^N$. Due to the constant right hand side, the POD equation (15) admits an explicit expression of the solution

$$\bar{M}\theta = E\bar{M}\theta_0 + (E - I)\bar{M}\bar{A}^{-1}\bar{b}$$

in terms of the matrix exponential $E = \exp(t\bar{A}\bar{M}^{-1})$, which allows a highly efficient evaluation of simulated temperatures $\vartheta(t) \approx V\theta(t)$ at given measurement times.

Posterior structure. Using the reduced POD model for evaluating posterior π_{post} a sampling $S = (p_i)_{1 \le i \le N_S}$ of the posterior distribution of size $N_S = 8 \cdot 10^6$ has been created using the Metropolis-Hastings algorithm with a Gibbs sampler [28].

In terms of the maximum posterior estimate p_{MAP} and estimated covariance $\Gamma(\vartheta^m)$ on the one hand and the sample mean $E[S] = N_S^{-1} \sum_{i=1}^{N_S} p_i$ and sample covariance $\text{Cov}[S] = (N_S - 1)^{-1} \sum_{i=1}^{N_S} (p_i - E[S])(p_i - E[S])^T$ on the other hand, the relative deviation of mean and covariance is small,

$$\frac{\|p_{\text{MAP}} - E[S]\|_{\text{Cov}[S]^{-1}}}{\|E[S]\|_{\text{Cov}[S]^{-1}}} \le 0.01, \qquad \frac{\|\Gamma(\vartheta^m) - \text{Cov}[S]\|}{\|\text{Cov}[S]\|} \le 0.15,$$

which suggests that local uncertainty quantification should provide reasonably accurate values.

This is also supported by the histograms of marginal densities derived from the sampling and shown in Figure 2 agreeing very well with a normal distribution.

3.3 Numerical example

Let us investigate how much the acquisition of more than one temperature measurement can improve the accuracy of the estimated time of death, evaluated

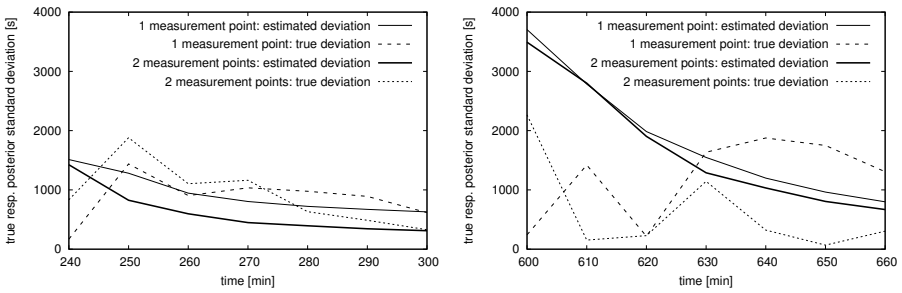

Figure 3: Estimated marginal posterior standard deviation from local uncertainty quantification for both protocols (solid lines), and absolute estimation error for a measurement sequence drawn from the likelihood distribution (dotted lines). *Left:* true ToD = 4 h. *Right:* true ToD = 10 h.

in terms of marginal posterior standard deviation. As fictitious measurement protocols we choose (a) sequential acquisition of rectal temperature every ten minutes and (b) simultaneous rectal and skin temperature measurements at sequential time points every ten minutes. For the latter, an arbitrary skin position in the ventral pelvic region has been chosen.

For the generation of artificial measurement data, material parameters have been drawn randomly from their respective prior distributions, with temperatures recorded starting at a time of death $T = 4h$ and $T = 10h$. The heat equation (4) has been solved with a finer discretization in time and space for measurement generation than for inversion, avoiding an inverse crime [15].

Estimated time of death and its approximate standard deviation as obtained from local uncertainty equation is shown in Figure 3. The accuracy improvement by a factor of four resulting from acquiring several more measurements is clearly visible. This is in contrast to previous findings in [13], where barely any improvement and even deterioration of variance estimates have been observed, and in [29], where three measurements starting at $T = 1.75$ h after death resulted in too small time of death estimates of mean 0.83 h in twenty cases – an average error of more than 50%. The reason appears to be that both papers rely on the phenomenological Marshall-Hoare model, which is not comprehensive enough to describe the actual cooling curves accurately, and that [13] is based on a simple averaging of multiple ToD estimates computed independently from single measurements. Thus, a sufficiently rich forward model able to capture the physical cooling processes in combination with a proper inverse problem approach seems to be necessary to exploit the additional information contained in multiple temperature measurements.

While taking more rectal measurements sequentially in time improves the uncertainty estimate considerably, the additional benefit of the second spatial location depends strongly on the time of death, being rather small for larger times of death. This will be confirmed by the design of experiments in Section 4 below.

Apparently, solving an inverse problem based on a mechanistic forward problem for multiple temperature measurements is a promising way for improving the accuracy of the estimation compared to current practice. Since the ac-

quisition of measurements on the crime scene incurs an additional effort, the immediate question is which measurement protocol provides the best accuracy for a given budget of measurements that can be taken. This problem of design of experiments is addressed in the next section.

4 Optimal Design of Experiments

4.1 DoE problem

A measurement protocol (or design) is a finite set $M \subset \mathbb{R}_+ \times \Omega$ of measurement points (τ_i, x_i). For simplicity reasons, we choose spatial measurement points from a discrete set $\bar{X} \subset \Omega$ of $\bar{m}_x$ candidate locations that are defined in view of their practical accessibility. The measurement effort on the crime scene is only determined by the number of different spatial measurement locations and the total measurement time, since with suitable equipment it makes no difference how many measurements a placed probe takes within the given time frame. Assuming sequential measurements to be taken every ten minutes, we will therefore consider designs of the form

$$M = \mathcal{T} \times X, \quad X \subset \bar{X}, \quad \mathcal{T} = \{hi \mid i = 0, \dots, m_t - 1\}, \quad h = 600\,\mathrm{s}.$$

For a given budget of effort, given in terms of measurement time frame m_t and number $m_x = |X|$ of measurement locations, the choice of measurement protocol should be made such as to minimize the resulting local uncertainty estimate $\Gamma(\vartheta^m, M)_{TT} = (J''(p_{\mathrm{MAP}}; \vartheta^m)^{-1})_{TT}$, which now depends not only on the measurements ϑ^m but also on the design M, and in particular on X.

Equivalently, the design M can be formulated in terms of binary weights $w \in \{0,1\}^{\bar{m}_x}$ for the candidate locations, with $w_i = 1 \Leftrightarrow x_i \in X$, and $\mathbb{1}^T w = m_x$. Sorting the measurement points (τ_i, x_i) by spatial location x, the likelihood information matrix Σ_l^{-1} has to be replaced by $W\Sigma_l^{-1}W$, where $W = \mathrm{diag}(w) \otimes I \in \mathbb{R}^{m_x m_t \times m_x m_t}$ is the diagonal matrix with entries w_i occuring m_t times each, see, e.g., [1, 2].

Of course, when choosing the design M, the measurements ϑ^m and consequently p_{MAP} are still unknown. We first consider only a local optimal design for the a priori most likely outcome, i.e.,

$$p_{\mathrm{prior}}(T_{\mathrm{prior}}) = (T_{\mathrm{prior}}, E[\pi_{\mathrm{prior}}(\ln(\rho c_{\mathrm{bone}}))], \dots, E[\pi_{\mathrm{prior}}(\ln \gamma)]) \tag{16}$$

and $\vartheta^m = F(p_{\mathrm{prior}})$. Note that $\pi_{\mathrm{prior}}(T)$ tends to have the largest coefficient of variation among the marginal prior distributions, such that a fixed choice $T_{\mathrm{prior}} = E[\pi_{\mathrm{prior}}(T)] = (t_a + t_b)/2$ will often be misleading. We therefore consider p_{prior} to be parametrized over T_{prior} and address the variation of T_{prior} later on.

The local posterior covariance approximation (14) then reads

$$\Gamma(w, T_{\mathrm{prior}})^{-1} = F'(p_{\mathrm{prior}}(T_{\mathrm{prior}}))^T W \Sigma_l^{-1} W F'(p_{\mathrm{prior}}(T_{\mathrm{prior}})) + \Sigma_p^{-1}, \tag{17}$$

with the posterior marginal standard deviation of the time of death,

$$\sigma_T(w, T_{\mathrm{prior}}) = \Gamma(w, T_{\mathrm{prior}})_{TT}^{1/2},$$

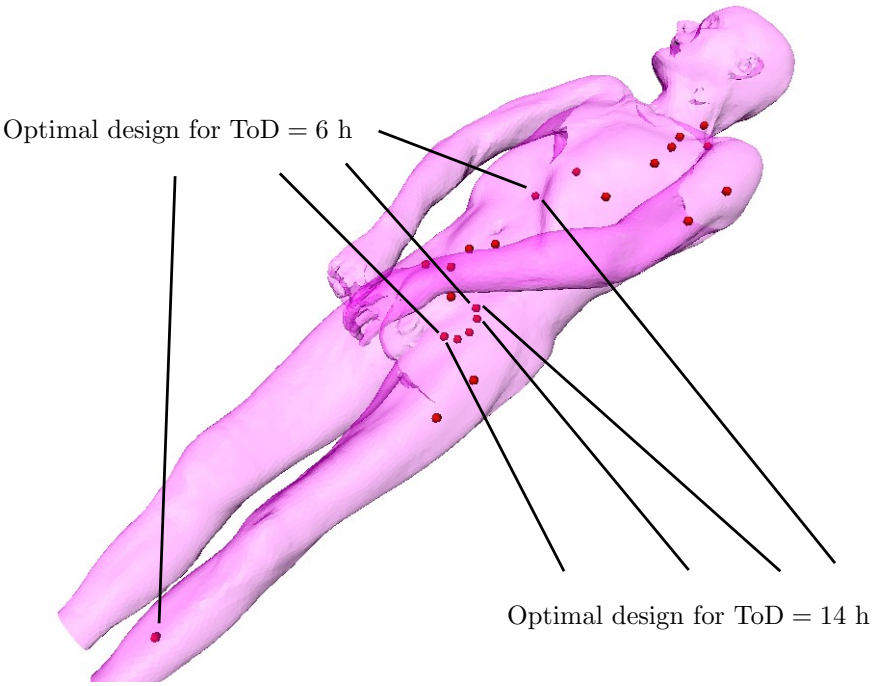

Figure 4: Set $\bar{X}$ of candidate locations for measurements. Interior: Five rectal points, two points at the liver. Surface: three points on the leg, two points at the shoulder, four points on the chest, two points at the throat, five points at the stomach. Spatial measurement locations of optimal designs with $m_x = m_t = 4$ for $T_{\text{prior}} \in \{6\,\text{h}, 14\,\text{h}\}$ are indicated.

as the ultimate quantity of interest. The optimal design of experiments problem is thus

$$\min_{w \in \{0,1\}^{\bar{m}_x}} \sigma_T \quad \text{subject to} \quad \mathbb{1}^T w = m_x. \tag{18}$$

The integer requirement $w \in \{0,1\}^{\bar{m}}$ makes the DoE problem (18) NP-hard [23]. Its solution by complete enumeration is only possible for small numbers $\bar{m}_x$ and m_x. The continuous relaxation $w \in [0,1]^{\bar{m}}$, in contrast, can be solved efficiently by nonlinear programming solvers also for larger $\bar{m}_x$ and m_x. Feasible but suboptimal integer solutions can then be obtained by rounding. Globally optimal solutions can be obtained at higher cost by mixed integer programming approaches like branch and bound.

4.2 Numerical experiments

In order to limit the computational complexity, we select $\bar{m}_x = 23$ mostly easily accessible spatial positions shown in Figure 4, of which five are located inside the rectum, 16 distributed on the skin surface, and two inside the liver.

Within this setting, we will explore the potential benefit of a systematic optimal design of experiments compared to both, the current practice of taking only one rectal temperature measurement, and the ad hoc design used in Sec-

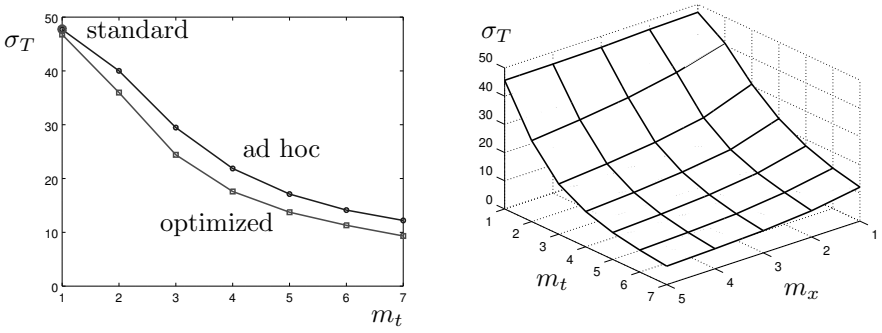

Figure 5: Expected standard deviation σ_T [min] of the time of death estimate for different designs, at $T_{\text{prior}} = 10\,\text{h}$. *Left:* Comparison of ad hoc design from Section 3.3 and optimal design with $m_x = 2$ for up to one hour of measurement. For reference, the standard design (one rectal measurement) is shown as well. *Right:* Optimal designs for up to five spatial locations and up to one hour of measurement.

tion 3.3, as well as the dependence of design and improvement on the actual time of death T.

Expected benefit of optimal designs. In the setting of Section 3.3 with $T_{\text{prior}} = 10\,\text{h}$, we consider up to five measurement locations and up to an hour measurement time, i.e., $m_x \leq 5$ and $m_t \leq 7$. The estimated standard deviation σ_T of the time of death estimate is shown in Figure 5 for the standard method, the ad hoc design from Section 3.3, and the globally optimal design for different values of m_x and m_t.

Obviously, there is a small but noticeable improvement of expected estimation error in the order of 5 min (about 20%) visible in Figure 5, left, when moving from the ad hoc design to an optimized design with $m_x = 2$ measurement locations. The improvement is much less pronounced if only one or two sequential measurements in time are taken. Altogether, an expected error of around 10 min is achieved, five times less than the standard design. Adding more spatial locations in Figure 5, right, improves the expected error further, down to about 6 min. Taking more sequential measurements appears to be more important than increasing the number of measurement locations, though.

The high accuracy estimated in this numerical example, with a standard deviation of time of death of only 6 min, is probably too optimistic compared to practical situations, since several model uncertainties have been treated in a cursory way by simply increasing the likelihood bias term. The biases of measurements in different spatial locations, however, are assumed to be independent, even if the locations are near to each other. This is certainly appropriate for independent temperature probes or independent placement of probes, but not for global effects like varying environmental temperature. While the impact of independent bias sources can be reduced by using more temperature probes, e.g., placing several in nearby rectal locations, the global bias will stay – which is not captured by the simple likelihood used here.

Some resulting designs are shown in Figure 4. As might be expected, the de-

signs are quite stable with respect to changing m_x or m_t, i.e., if m_x is increased, most of the time there is a new location added, without further exchanges of locations. For different values of m_t, the optimal designs are mostly the same, with an occasional exchange of nearby locations. A remarkable observation is that up to design size six, only locations in the interior are selected, even though their cooling curves are closely correlated. One reason is that despite the temperature correlation, the bias of different probes is assumed to be independent, such that using more probes, even in the same location, reduces the measurement error. The other reason is that after $T = 10\,\mathrm{h}$, the skin is already too much cooled to provide useful temperature information. This will be different for smaller values of T, or in situations where parts of the skin are thermally isolated due to clothing or ground contact. We may therefore expect different designs in other situations, which we explore next.

Dependence of optimal designs on the time of death. The choice of the design point p_{prior} in (16) is natural only for the thermal parameters in p_{prior}, but not for the time of death T_{prior}. We therefore investigate how the optimal designs and the expected uncertainty depends on T_{prior} and the actual time of death T in the usual case $T \neq T_{\text{prior}}$.

We computed optimal designs for $m_x = m_t = 4$ for different choices of $T_{\text{prior}} \in [2\,\mathrm{h}, 14\,\mathrm{h}]$ and estimated the expected time of death standard deviation σ_T for different actual times $T \in [1\,\mathrm{h}, 16\,\mathrm{h}]$. The resulting designs for $T_{\text{prior}} \in \{6\,\mathrm{h}, 14\,\mathrm{h}\}$ are shown in Figure 4. As expected, optimizing for very short times of death considers only surface locations, since the interior points have not yet started cooling down sufficiently. For medium times, skin and interior locations are mixed, whereas for longer times only interior locations are chosen.

The impact on the expected estimation accuracy is shown in Figure 6. Obviously, the design optimized for a particular value of T_{prior} is the best design at $T = T_{\text{prior}}$. Clearly, none of the single optimal designs is optimal for the whole range of possible times T of death. One way to address this is a sequential design approach: With a first rectal measurement, a provisional estimate $\hat{T}$ is obtained, and then a design selected and applied that has been optimized for some T_{prior} close to $\hat{T}$, achieving nearly optimal accuracy at the expense of fixing a design only after the first measurement. A different way is to consider Bayesian design of experiments at least for T_{prior}, which is done below.

Robust and Bayesian design. An alternative to a sequential design is to look for a design $w \in \{0,1\}^{\bar{m}_x}$ that is either optimal on average, or optimal in the worst case, leading to Bayesian optimal design [6] or robust design [24]. For the average case, we consider the uncertainty of a design w to be either

$$\begin{aligned} U^1_{\text{abs}}(w) &= \int_{T_{\text{prior}} \in \mathbb{R}_+} \sigma_T(w, T_{\text{prior}})\, d\pi_{\text{prior}}(T_{\text{prior}}) \\ &= \frac{1}{t_b - t_a} \|\sigma_T(w, T_{\text{prior}})\|_{L^1([t_a,t_b])} \end{aligned}$$

or

$$U^1_{\text{rel}}(w) = \frac{1}{t_b - t_a} \left\| \frac{\sigma_T(w, T_{\text{prior}})}{T_{\text{prior}}} \right\|_{L^1([t_a,t_b])}.$$

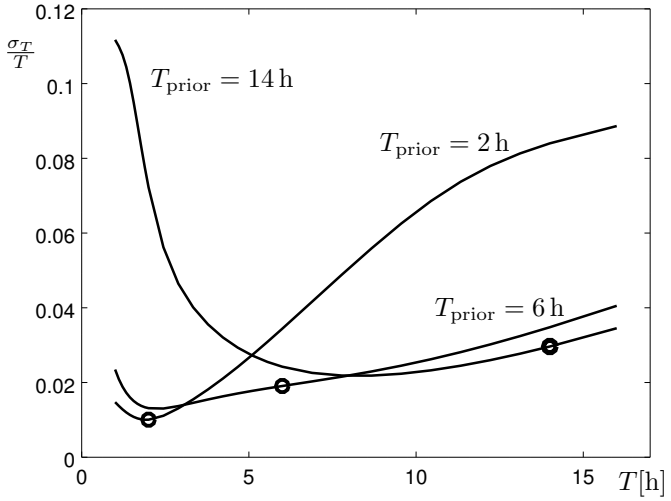

Figure 6: Dependence of expected relative estimation error σ_T/T on T_{prior} versus the actual time of death T.

For the robust case, we simply replace the L^1-norm by the L^∞-norm and obtain U^∞_{abs} and U^∞_{rel}. Minimizing U then provides four designs that are reasonable for a wide range of times T of death.

Here we fix $t_a = 1\,\text{h}$, $t_b = 16\,\text{h}$, and $m_t = m_x = 4$, for computing the four designs w^1_{abs}, w^∞_{abs}, w^1_{rel}, and w^∞_{rel}. The expected error σ_T grows with T, such that minimizing the absolute uncertainty σ_T results in designs that are optimized for large T and hence contain only interior points. As the optimization essentially focuses only on the largest time considered, and there are relatively few interior points to choose from, it is not surprising that the two designs w^1_{abs} and w^∞_{abs} coincide. In contrast, the relative error notion leads to designs differing in the choice of the one surface measurement location included in the designs. Since surface locations mainly affect the result for smaller values of T, the two designs perform almost equal for large times of death.

The expected estimation errors are plotted against the actual time of death T in Figure 7.

5 Conclusions

The numerical results presented above strongly support the following four main findings of the paper.

First, local uncertainty quantification based on linearization around the maximum posterior point estimate in a Bayesian setting appears to be sufficiently accurate to assess and compare the reliability of time of death estimates. The agreement of Taylor-based Gaussian approximation and Monte-Carlo sampling of the posterior distribution is quite good in the setting considered here.

Second, model reduction by proper orthogonal decomposition is a valuable and sufficiently accurate tool in particular for uncertainty quantification. It

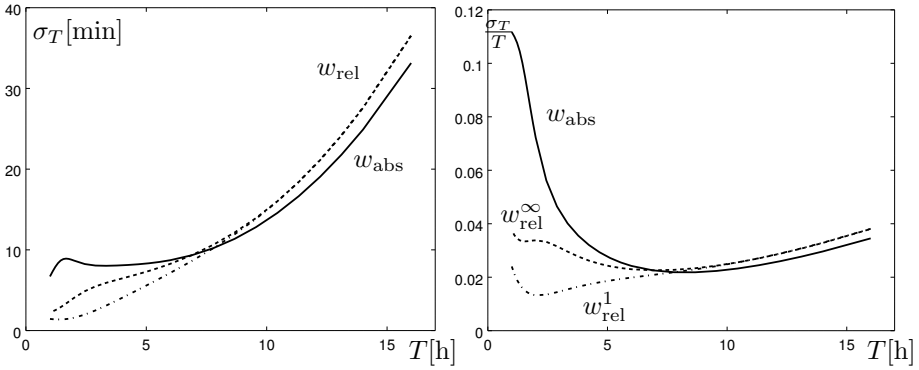

Figure 7: Bayesian and robust designs $w^1_{\text{abs}} = w^\infty_{\text{abs}}$, w^1_{rel}, and w^∞_{rel} for absolute and relative error concepts. *Left:* Standard deviation σ_T verus T. *Right:* Relative standard deviation σ_T/T versus T.

allows to perform Monte-Carlo sampling of the posterior density, which is not affordable with finite element solvers, and simplifies uncertainty quantification and Bayesian optimal design of experiments. While ten modes appear to be enough for uncertainty quantification and design of experiments, its use for actual estimation will require more modes.

Third, acquiring more temperature measurements can improve the expected accuracy of time of death estimates considerably compared to current practice. In the setting considered here, the standard deviation of the time of death estimate could be reduced from about 50 min to about 10 min for a time of death of 10 h. Even though the actual values are somewhat optimistic, since several model uncertainties have been included only in a cursory way, we expect the improvements to be significant in more complex settings. The exploitation of several measurements requires that the underlying forward model is able to reproduce actual cooling curves faithfully. This is a clear advantage of mechanistic models over simpler phenomenological models. Mechanistic models also allow the straightforward inclusion of multiple spatial measurement locations, which is hard to achieve with phenomenological models.

Finally, optimal design of experiments is a viable and promising approach to come up with practical and accurate measurement protocols that improve the accuracy over ad hoc designs with multiple measurements. It also reveals the importance of different spatial measurement locations for the estimation accuracy for different actual times of death.

Acknowledgement. We thank our colleague Marian Moldenhauer for careful reading of the article and for helpful comments. Partial funding by University of Jena is gratefully acknowledged.

References

[1] A. Alexanderian, N. Petra, G. Stadler, and O. Ghattas. A-Optimal Design of Experiments for Infinite-Dimensional Bayesian Linear Inverse Problems

with Regularized L_0-Sparsification. *SIAM J. Sci. Comput.*, 36:2122–2148, 2014.

[2] A. Alexanderian, N. Petra, G. Stadler, and O. Ghattas. A Fast and Scalable Method for A-Optimal Design of Experiments for Infinite-dimensional Bayesian Nonlinear Inverse Problems. *SIAM J. Sci. Comput.*, 38:243–272, 2016.

[3] I. Bauer, S. Körkel, H.G. Bock, and J.P. Schlöder. Optimale Versuchsplanung für nichtlineare Prozesse. In *Schriftliche Projektpräsentation zum BMBF-Verbundvorhaben*. DECHEMA e.V., 1998.

[4] J.O. Berger. *Statistical Decision Theory and Bayesian Analysis*. Springer, 2013.

[5] Y.A. Cengle and A.J. Ghajar. *Heat and Mass Transfer*. McGraw-Hill Education, 2015.

[6] K. Chaloner and I. Verdinelli. Bayesian experimental design: A review. *Statist. Sci.*, 10(3):273–304, 1995.

[7] Arbeitsgemeinschaft der Wissenschaftlichen Medizinischen Fachgesellschaften. Leitlinien der Deutschen Gesellschaft für Rechtsmedizin, 2017. Accessed: 01-01-2018, Available at http://www.awmf.org/leitlinien/detail/ll/054-002.html.

[8] P. Deuflhard. *Newton Methods for Nonlinear Problems*. Springer, 2011.

[9] P. Deuflhard and M. Weiser. *Adaptive numerical solution of PDEs*. de Gruyter, 2012.

[10] S. Götschel, M. Weiser, and A. Schiela. Solving optimal control problems with the Kaskade 7 finite element toolbox. In A. Dedner, B. Flemisch, and R. Klöfkorn, editors, *Advances in DUNE*, pages 101–112. Springer, 2012.

[11] C. Henßge. Death time estimation in case work. I. The rectal temperature time of death nomogram. *Forensic Sci. Int.*, 38:209–236, 1988.

[12] C. Henßge and B. Madea. Estimation of the time since death in the early post-mortem period. *Forensic Sci. Int.*, 144:167–175, 2004.

[13] M. Hubig, H. Muggenthaler, S. Schenkl, and G. Mall. Do multiple temperature measurements improve temperature-based death time estimation? The information degradation inequality. *Int. J. Legal Med.*, 130:1243 – 1251, 2016.

[14] M. Hubig, H. Muggenthaler, I. Sinicina, and G. Mall. Temperature-Based Forensic Death Time Estimation: The Standard Model in Experimental Test. *Legal Med.*, 17:381–387, 2015.

[15] J. Kaipio and E. Somersalo. *Statistical and Computational Inverse Problems*. Springer, 2010.

[16] S. Körkel and E. Kostina. Numerical methods for nonlinear experimental design. In H. G. Bock, E. Kostina, H. X. Phu, and R. Rannacher, editors, *Modelling, Simulation and Optimization of Complex Processes*, pages 255–272. Springer, 2004.

[17] K. Kunisch and S. Volkwein. Galerkin proper orthogonal decomposition methods for parabolic problems. *Num. Math.*, 90(1):117–148, 2001.

[18] E. Limpert, W.A. Stahel, and M. Abbt. Log-normal distributions across the sciences: Keys and clues. *BioScience*, 51(5):341–352, 2001.

[19] G. Mall and W. Eisenmenger. Estimation of Time since Death by heat-flow Finite-Element model. Part I: Method, Model, Calibration and Validation. *Legal Med.*, 7:69–80, 2005.

[20] T. Marshall and F. Hoare. Estimating the time of death: the rectal cooling after death and its mathematical expression. *J. Forensic Sci.*, 7:56–81, 1962.

[21] H. Muggenthaler, M. Hubig, S. Schenkl, S. Niederegger, and G. Mall. Calibration and Parameter Variation Using a Finite Element Model for Death Time Estimation: The Influence of the Substrate. *Legal Med.*, 25:23–28, 2017.

[22] H. Muggenthaler, I. Sinicina, M. Hubig, and G. Mall. Database of post-mortem rectal cooling cases under strictly controlled conditions: a useful tool in death time estimation. *Legal Med.*, 126:79–87, 2012.

[23] B. K. Natarajan. Sparse Approximate Solutions to Linear Systems. *SIAM J. Comput.*, 24:227–234, 1995.

[24] G.-J. Park, T.-H. Lee, K.H. Lee, and K.-H. Hwang. Robust design: An overview. *AIAA J.*, 44(1):181–191, 2006.

[25] H.H. Pennes. Analysis of tissue and arterial blood temperatures in the resting human forearm. *J. Appl. Phys.*, 1:93–122, 1948.

[26] R. Pinnau. Model reduction via proper orthogonal decomposition. In W.H.A. Schilders, H.A. van der Vorst, and J. Rommes, editors, *Model Order Reduction: Theory, Research Aspects and Applications*, pages 95–109. Springer, 2008.

[27] F. Pukelsheim. *Optimal Design of Experiments*. SIAM, 1993.

[28] C.P. Robert and G. Casella. *Monte Carlo Statistical Methods*. Springer, 2004.

[29] M. Rodrigo. A Nonlinear Least Squares Approach to Time of Death Estimation Via Body Cooling. *J. Forensic Sci.*, 61:230–233, 2016.

[30] S. Schenkl, H. Muggenthaler, M. Hubig, B. Erdmann, M. Weiser, S. Zachow, A. Heinrich, F.V. Güttler, U. Teichgräber, and G. Mall. Automatic CT-based Finite Element Model Generation for Temperature-based Death Time Estimation: Feasibility Study and Sensitivity Analysis. *Int. J. Legal Med.*, 131(3):699 – 712, 2017.

[31] M. Weiser, B. Erdmann, S. Schenkl, H. Muggenthaler, M. Hubig, G. Mall, and S. Zachow. Uncertainty in Temperature-Based Determination of Time of Death. Technical report, Zuse Institute Berlin, 2017.

[32] S. Zachow, M. Zilske, and H.-C. Hege. 3D Reconstruction of Individual Anatomy from Medical Image Data: Segmentation and Geometry Processing. Technical report, Zuse Institute Berlin, 2007.

[33] O. Zienkewicz, R. Taylor, and J.Z. Zhu. *The Finite Element Method: Its Basis and Fundamentals*. Butterworth-Heinemann, 2013.